HYDROLOGICAL PROCESSES
Hydrol. Process. (2015)
Published online in Wiley Online Library
(wileyonlinelibrary.com) DOI: 10.1002/hyp.10535

SAS2: the system for acoustic sensing of snow

N. J. Kinar* and J. W. Pomeroy
Centre for Hydrology, University of Saskatchewan, Canada

Abstract:

A novel electronic sensing system (SAS2) was designed to non-invasively and simultaneously measure snow density, liquid water content, and temperature of snow using acoustics and obtain images of the snowpack. The system is an updated and more sophisticated version of previous acoustic sensing systems, and this paper presents an update on the development of acoustic sensing methods to measure multiple snowpack properties and obtain images of snowpack stratigraphy. Air-coupled acoustic waves were sent into and reflected from the snowpack by the SAS2 system. An inverse model based on a modified version of the Biot–Stoll theory of sound propagation through porous media was used to obtain acoustic measurements of snow and images of the snowpack. The SAS2 was deployed at ten field sites in the Canadian Rockies. Stationary and portable versions of the system were deployed and tested. This paper reports initial tests of the SAS2 that were conducted at the field sites to compare acoustic model outputs with gravimetric measurements of snow density, dielectric measurements of liquid water content, and thermocouple and thermometer measurements of snow temperature. Snow water equivalent could be estimated more accurately and quickly with the SAS2 than with an ESC30 gravimetric snow tube. Unlike monopulse sonar and radar sensors, the SAS2 utilizes a continuous-wave Maximum Length Sequence (MLS) that is more robust to environmental noise. The SAS2 serves as a proof-of-concept of the acoustic snow measurement technique with potential for further research as identified and discussed in this paper. Copyright © 2015 John Wiley & Sons, Ltd.

KEY WORDS acoustics; snowpack; snow density; snow liquid water content; snow temperature; snow water equivalent

Received 8 November 2014; Accepted 1 May 2015

INTRODUCTION

Snow water equivalent (SWE) is a key hydrological state variable that strongly indicates the potential for streamflow generation and infiltration to soils (Gray *et al*., 2001; Mote, 2003; Barnett *et al*., 2005; Male and Gray, 1981). SWE can be found from snow density and depth, but both properties vary substantially with space and time and so the rapid measurement of SWE to aid in characterization of snowpack dynamics has been a long term goal in snow hydrology (Pomeroy and Gray, 1995). Liquid water content and temperature are two important snowpack state variables that indicate the proportion of liquid *versus* solid water and the thermal state of the snowpack—they are key to estimating internal energy state and the ripeness of the snowpack for snowmelt estimation. These variables are all used in studies of snowpack evolution for hydrology (Pomeroy *et al*., 2007), atmospheric science (Bartlett *et al*., 2006), and ecology (Jones *et al*., 2011). Snow metamorphism (Colbeck, 1982), the rate of water transport through snow (Colbeck, 1972, 1974a,b, 1975, 1977; Williams *et al*., 2010; McGurk and Marsh, 1995; Techel and Pielmeier, 2011), and snowmelt (Ferguson, 1999; Ellis *et al*., 2013; Gray and Landine, 1988) are also related to these variables.

However, most methods used to determine SWE, snow density, liquid water content, and temperature require invasive destruction of the snowpack, insertion of probes into the snowpack, or pre-snowpack formation placement of instrumentation and are time-consuming or difficult to perform. As a result, there is no single widely accepted set of techniques that can be used to simultaneously and non-invasively measure the density, liquid water content, and temperature of a seasonal snowpack. Moreover, snow sampling and the creation of a snowpit is a laborious process that is time-consuming, invasive, and prone to human error.

SWE and snow density have been measured by the use of acoustics. Kinar and Pomeroy (2007) utilized a single loudspeaker and microphone to send sound waves into the snowpack. Kinar and Pomeroy (2008a,b) and Kinar and Pomeroy (2009) later used a Maximum Length Sequence (MLS) as the source signal and built an electronic circuit to perform automated acoustic sensing of snow.

The objectives of this paper are to describe and evaluate an active sensing technique that can obtain images of the snowpack while simultaneously and non-invasively measuring snow density, liquid water content, and temperature by the use of acoustic waves produced in the air medium and coupled into the snowpack. The

*Correspondence to: N. J. Kinar, Centre for Hydrology, University of Saskatchewan, 117 Science Place, Saskatoon, Saskatchewan, S7N 5C8, Canada.
E-mail: n.kinar@usask.ca

technique is based on a model of sound propagation in snow, the Unified Thermoacoustic Model (UTAM) that takes into consideration changes in temperature and liquid water content. A novel electronic sensing system was created to deploy the active sensing technique—the System for Acoustic Sensing of Snow (SAS2).

THEORY

UTAM model

Following Johnson (1982), Kinar and Pomeroy (2007), and Kinar and Pomeroy (2008a,b), we assume that snow is a porous medium comprised of an ice frame with pore spaces; the porous medium is composed from snow particles that have been subjected to snow metamorphism. We consider a slow P-wave propagating in the pore spaces of the snowpack as being important for acoustic sampling of snow.

Stoll (1985) modified Biot's theory so that it is physically realizable (Stoll, 1979, 1980, 1985, 2002; Stoll and Bryan, 1970; Stoll and Kan, 1981). However, the Biot–Stoll equations do not completely describe an acoustic model of snow. Naturally occurring snow is a multiphase porous medium comprised of an ice frame filled with a mixture of air as a gas and water as a fluid (Colbeck, 1997). This 'mixture theory' approach has been used in models of snowpack evolution (Morland *et al.*, 1990; Morris and Kelly, 1990) and is used here in this section to modify the equations given by Stoll (1985).

The volume fraction of air ε_a, the volume fraction of water ε_w, and the effective fluid density ρ_f in the pore spaces of the snow medium are calculated using the following derivation, where V_a is the volume of air, V_w is the volume of water in a control volume V_T, and ρ_a, ρ_w are the densities of air and water:

$$\phi = \frac{V_a + V_w}{V_T}$$

$$\varepsilon_a + \varepsilon_w = 1$$

$$\varepsilon_a = \frac{V_a}{V_a + V_w}$$

$$\theta_w = \frac{V_w}{V_T}$$

$$\theta_a = \frac{V_a}{V_T}$$

$$\varepsilon_a = \frac{1}{1 + \frac{\theta_w}{\theta_a}}$$

$$\varepsilon_w = \frac{V_w}{V_a + V_w}$$

$$\varepsilon_w = \frac{1}{1 + \frac{\theta_a}{\theta_w}}$$

$$\rho_f = \varepsilon_a \rho_a + \varepsilon_w \rho_w.$$

In the above equations, ϕ is the snowpack porosity, ε_a is the volume fraction of air in the pore space of the snowpack, ε_w is the volume fraction of water, θ_w is the liquid water content, θ_a is the air fraction as the 'air porosity,' and ρ_f is the fluid density of the air and water in the pore spaces of the snowpack.

Assuming that the volumes of air (V_a), ice (V_i), and water (V_w) are fractional constituents of V_T, the air porosity θ_a, liquid water content θ_w, and ice fraction θ_i are given by (Bartelt and Lehning, 2002):

$$\theta_i = \frac{V_i}{V_T}$$

$$\theta_a + \theta_w + \theta_i = 1.$$

Percolation theory (Grimmett, 1999) was used to compute the Young's modulus E and shear modulus G of snow. Percolation theory provides a macroscopic, mathematically rigorous model of connectivity in a porous medium. Following Phani and Niyogi (1987), the Young's modulus and shear modulus of the snow porous material was related to porosity using Kováčik's (1999) equations.

To compute Young's modulus E and shear modulus G of snow using percolation theory, Young's modulus E_0 and shear modulus G_0 of the solid frame comprising the Biot-type medium are taken to be similar to ice. The moduli of ice are computed using theory given by Petrenko and Whitworth (2002) and are calculated as a function of snow temperature T. The bulk modulus of snow K_b is then calculated from E and G. The bulk modulus of the sediment comprising the frame K_r is taken to be similar to ice and computed in a similar fashion.

To compensate for viscoelastic losses in the porous medium, the shear modulus μ used in the Biot–Stoll equations is taken as a complex value, defined by Albert (1993) as:

$$\mu = G(1 + i\delta).$$

The real-valued shear modulus is G, a complex number is represented by $i = \sqrt{-1}$, and δ is the dimensionless loss tangent that models the dissipation of acoustic waves in the porous medium (Stoll, 1989).

To calculate the density of air ρ_a in the snowpack, the air is assumed to be an ideal gas with temperature T. Although water vapour and the mole fraction of gases in air will influence ρ_a, the ideal gas assumption is applied here because it is useful in the absence of any other information.

Using the mixture theory approach and assuming that the bulk modulus of the snow mixture is related in a similar fashion to parallel resistors, the effective bulk modulus is calculated using the theory of Rau and Chaney (1988). The bulk modulus of water is calculated from the Newton–Laplace equation (Raichel, 2006) that is used in

acoustics to determine the speed of sound in water given the water density ρ_w. The speed of sound in water is calculated using the empirical equation given by Bilaniuk and Wong (1993, 1996). The density of water ρ_w is computed using theory developed by Tanaka *et al*. (2001).

Using a mixture theory approach, the effective density ρ of the snowpack medium is calculated (Bartelt and Lehning, 2002):

$$\rho = \rho_s = \rho_a\theta_a + \rho_w\theta_w + \rho_i\theta_i$$
$$\theta_a = 1 - \theta_w - \theta_i.$$

Following Evje and Karlsen (2009), the viscosity η of the pore space fluid is also calculated using the mixture theory approach:

$$\eta = \varepsilon_w\eta_w + \varepsilon_a\eta_a.$$

The viscosity of water η_w in the pore spaces is calculated using an empirical equation given by Huber *et al*. (2009), whereas the viscosity of air η_a is computed using the Sutherland formula as a function of temperature (Anderson, 1991). The tortuosity α of the snowpack is estimated using the theory of Berryman (1980), following Kinar and Pomeroy (2007, 2008a,b, 2009) using a dimensionless shape factor γ.

Inverse model

The UTAM serves as a forward model because physical properties of snow are mathematically related to the speed and attenuation of sound waves. An inverse model determines three unknowns from the speed and attenuation calculated by the Biot–Stoll equations: the porosity ϕ, liquid water content θ_w, and temperature T of snow within a control volume. Given speeds and acoustic wave attenuations that are averaged over the depth of the snowpack, an equivalent one-layer inverse model computes the $\{\overline{\phi}, \overline{\theta}_w\overline{T}\}$ variables. The one-layer model was chosen because a multi-layer model was found to be ill-posed when used to find an inverse solution.

The idea behind the inverse model is similar to the Knott–Zoeppritz equations with angle-dependent reflection coefficients (Chavent, 2009; de Bruin *et al*., 1990). The speed of sound in snow is determined by a plane-wave destructor filter (Claerbout, 1992), whereas attenuation of sound waves in snow is measured by Q-analysis techniques in the spectrogram domain (Wang, 2004, 2008; Carrion and VerWest, 1987). The speed of sound in snow in the spectrogram domain is used for time-to-depth conversion for acoustic snow imaging. The speed of sound in the air from concomitant measurements of air temperature at the time of each acoustic measurement is used to determine the distance to the snow surface by kinematics. The useful frequency range of the speeds and attenuations was limited from 100 Hz to 10 kHz by the loudspeaker and microphone responses (Section System Description), and further research is required to determine if this range is also limited by snow structure and physical properties.

An interpolation algorithm similar to normal moveout (NMO) (Claerbout, 1992) is used to convert the sampled signals at each of the microphones to signals equivalent to spatial sampling at normal incidence. This permits long-term acoustic measurement of the snowpack with respect to changes in snow depth over time. A maximum cutoff depth limited by the duration of the source signal and measurements of snow depth is determined, and the discrete time-domain signal is appropriately truncated. This truncation is important with respect to obtaining images of snowpack stratigraphy. Acoustic scattering is incorporated into the inverse model using theory given by Kinar and Pomeroy (2008a).

Acoustic measurement model

The measurement system is placed above the surface of a snowpack and is comprised of a loudspeaker offset by 10.8 cm from six microphones with separation distances of 7.62 mm. The setup is similar to FMCW (Gubler and Hiller, 1984), bistatic sonar (Cox, 1989), and radar (Willis, 1991) systems (Figure 1). Separation distances and offsets were selected using a sensitivity analysis based on the physics of sound wave propagation in snow (Kinar, 2013). The effect of the height above the snow surface is discussed in Beam Footprint and Sampling Volume and is explicitly involved in the inverse model (Section Inverse Model).

Similar to sonar being reflected from a rough seabed (Lurton, 2002), buried vegetation and rough interfaces between layers will cause acoustic scattering (Kinar and Pomeroy, 2007, 2008a). Calculation of acoustic scattering for sound propagation in snow is discussed by Kinar and Pomeroy (2008a) and is incorporated into this model.

Following Kinar and Pomeroy (2009), the source signal is a continuous-wave Maximum Length Sequence (MLS) with a duration of 1.6 s. The Maximum Length Sequence (MLS) is not an impulsive acoustic source but is a chaotic, structured signal with high external noise immunity associated with the time-integrated signal energy of its waveform and its maximally flat bandwidth (Vanderkooy, 1994; Dunn and Hawksford, 1993; Rife and Vanderkooy, 1989). This makes the MLS robust to wind or anthropogenic noise such as a snow machine engine. The filter kernel of the snowpack is determined using a cross-correlation deconvolution algorithm (Borish and Angell, 1983; Rife and Vanderkooy, 1989). The response of the loudspeaker and acoustic effects of the enclosure case are removed using matched filtering. Lowpass filtering and decimation of the microphone signals are used to reduce spurious noise and reduce the amount of data for signal processing.

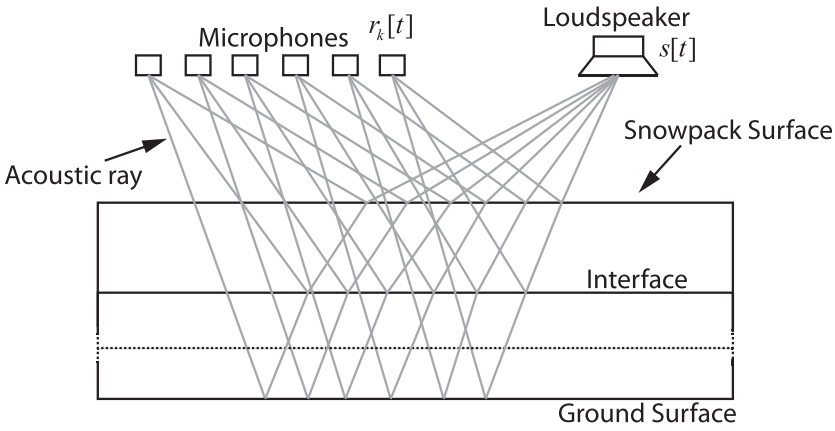

Figure 1. Conceptual diagram showing the acoustic measurement model. A loudspeaker is situated at an offset distance from six microphones. The signal sent from the loudspeaker is denoted as $s[t]$, and the signal received by a microphone is $r_k[t]$ for microphone number k where $1 \leq k \leq 6$. The dashed line represents that the snowpack can have more layers than shown in the conceptual diagram

Acoustic coupling of sound into snow

The impedance of the snow surface ξ_1 as a porous medium, as well as the sound pressure reflection coefficient Γ_1 of sound waves at the air–snow interface can be calculated as (Kinar and Pomeroy, 2007):

$$\xi_1 = \frac{\rho_0 c_0 \sqrt{\alpha_1}}{\phi_1}$$

$$\Gamma_1 = \frac{\rho_0 c_0 \sqrt{\alpha_1} - \phi_1 \rho_0 c_0}{\rho_0 c_0 \sqrt{\alpha_1} + \phi_1 \rho_0 c_0} = \frac{\sqrt{\alpha_1} - \phi_1}{\sqrt{\alpha_1} + \phi_1}.$$

The density of air is ρ_0, the speed of sound in air is c_0, the tortuosity is α_1, and the porosity is ϕ_1 for the first layer in the snowpack.

The sound pressure transmission coefficient is a measure of the acoustic energy that is transmitted between an air–snow interface and is computed as:

$$\psi_1 = 1 - \Gamma_1.$$

For reflections from successive snow–snow interfaces within the snowpack, the reflection coefficient Γ_k corresponding to an interface k within the snowpack is (Kinar and Pomeroy, 2007):

$$\Gamma_k = \frac{\phi_{k-1}\rho_0 c_0 \sqrt{\alpha_k} - \phi_k \rho_0 c_0 \sqrt{\alpha_{k-1}}}{\phi_{k-1}\rho_0 c_0 \sqrt{\alpha_k} + \phi_k \rho_0 c_0 \sqrt{\alpha_{k-1}}} = \frac{\phi_{k-1}\sqrt{\alpha_k} - \phi_k \sqrt{\alpha_{k-1}}}{\phi_{k-1}\sqrt{\alpha_k} + \phi_k \sqrt{\alpha_{k-1}}}.$$

The tortuosity of a snow layer is α_k, and the porosity is ϕ_k. For a reflection to occur between layers, it is assumed that $\alpha_k \neq \alpha_{k-1}$ and $\phi_k \neq \phi_{k-1}$. The corresponding transmission coefficient between two snow layers in the snowpack is:

$$\psi_k = 1 - \Gamma_k.$$

The reflection and transmission coefficients can be calculated using the shape factor γ and the porosity ϕ. The shape factor is assumed to range between $0.5 \leq \gamma \leq 0.67$ (Kinar and Pomeroy, 2008a). The porosity of seasonal snow is assumed to range between $0.40 \leq \phi \leq 0.89$.

Using this range of variables, the magnitude of the reflection coefficient ranges between $0.07 \leq \Gamma_1 \leq 0.56$ for an air–snow interface and $0.32 \leq \Gamma_1 \leq 0.44$ for a snow–snow interface. The corresponding transmission coefficient magnitudes range between $0.44 \leq \psi_1 \leq 0.93$ for an air–snow interface and $0.56 \leq \psi_k \leq 0.68$ for a snow–snow interface. This calculation suggests that sound waves sent from the SAS2 can enter the snowpack and can be used for acoustic characterization of snow.

DEVICES

System description

The **S**ystem for **A**coustic **S**ensing of **S**now (SAS2) was developed to autonomously send sound waves into snow and to receive reflections from the snowpack and is comprised of electronic circuit boards fastened inside of a waterproof enclosure case (Figure 2a–b). This is the second version of a snow acoustic sensing system that is to be distinguished from the first version reported by Kinar and Pomeroy (2009).

The sound power level of the loudspeaker as the sound source was determined to be 104 dB by measurements in an anechoic chamber (Room 2C96.1, Department of Electrical and Computer Engineering, University of Saskatchewan). Measurements were also made in the anechoic chamber to determine the frequency response of the loudspeaker, which ranged between 20 Hz and 20 kHz.

The microphone array is comprised of six digital microphones per row situated in an array of four rows for a total of 24 microphones. The frequency range of the

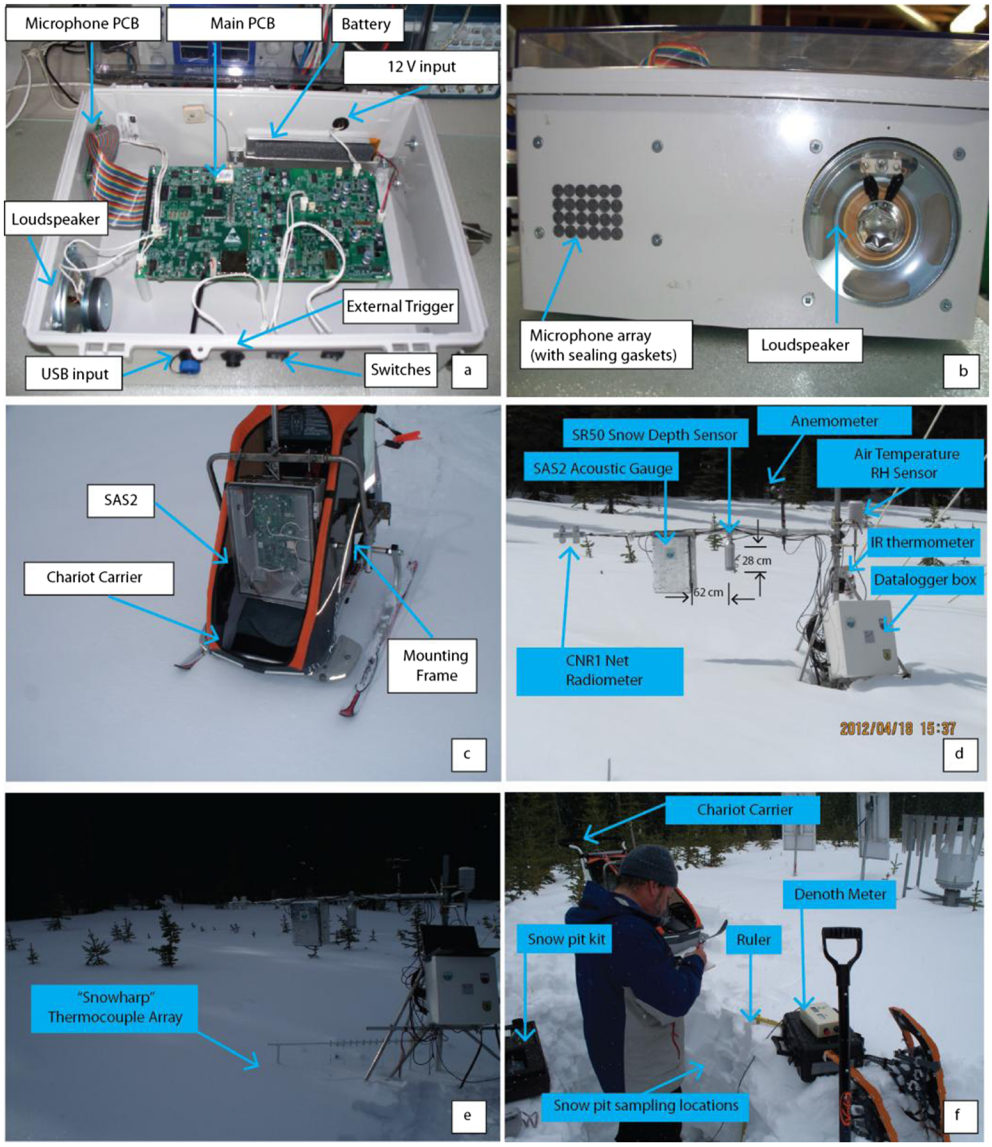

Figure 2. (a) Side view of the **S**ystem for **A**coustic **S**ensing of **S**now (SAS2) in an enclosure box. (b) Front view of the SAS2. (c) Portable deployment of the SAS2. (d) Stationary (met station) deployment of the SAS2. (e) Stationary SAS2 showing the top of the thermocouple array. (f) Snow pit sampling for testing of the SAS2. IR, infrared

microphones was characterized as 100 Hz to 10 kHz. The microphones were operated at a voltage of 3.3 V, and the digital sensitivity of these microphones was nominally −26 dBFS. An on-board processing system and associated circuitry collected data from the microphone array at a sampling rate of 2.1 MHz to ensure that the time of arrival of sound waves between microphones could be obtained at small offset distances. It is suspected that the holes in the enclosure case served as waveguides for incident sound pressure waves, but beam directionality is not precisely defined.

Two versions of the system were created: a portable version affixed to a modified Chariot© child carrier (Thule Inc., Calgary, Alberta, Canada) with skis (Figure 2c) and a stationary version fixed to mast arm (Figure 2d). The child carrier enabled the portable version of the SAS2 to be suspended above and moved over the snow surface. Acoustic measurements were triggered by pressing a button interfaced to the electronic circuit and attached to the child carrier push handle or pulling harness. Data collected during these experiments were stored by the circuit to an SD card.

Beam footprint and sampling volume

In a similar fashion to radar (Yankielun *et al.*, 2004), the footprint is the approximate area on the surface of the snowpack that is sensed by the microphone array. Assume

that the minimum half-width of the central lobe of the array is θ_m. For a lobe width of $\theta = \pm 43°$ calculated from theory given by Barger (1998) and Liu and Weiss (2010), the half-width for the SAS2 sensing system is $\theta_m = 43°$. Then, for SAS2 distances y_a above the snow surface of 5 cm $\leq y_a \leq$ 3 m observed during the collection of data used in this paper, the footprint ranges between 9 cm $\leq x_s \leq$ 5.6 m, as calculated using theory from Kinar and Pomeroy (2008a). For snow depths ranging between 3 cm and 2 m as reported in this paper (Table I), the effective sensing volume was computed using a recursive model (Kinar and Pomeroy, 2008a) as ranging between 150 cm^3 and 43 m^3.

Layer resolution

Assume that the source signal is comprised of a wavelet that propagates through the porous medium. This is true for an MLS after signal processing (Borish and Angell, 1983). Then an imaging resolution is established as (Widess, 1973):

$$\Delta y > \lambda_s/4$$
$$\lambda_s = c_s/f_a.$$

The minimum acoustic layer width is Δy, the wavelength of the sound wave in the snowpack is λ_s, the speed of the sound wave in snow is c_s, and the frequency of the sound wavelet is f_a. For a speed of sound in snow ranging between 10 m $s^{-1} \leq c_s \leq$ 331 m s^{-1} and 100 Hz $\leq f_a \leq$ 10 kHz for the bandwidth, the minimum acoustic layer width Δy that can be resolved is $\Delta y = 2.5 \times 10^{-4}$ m.

FIELD SITES, DEPLOYMENT, AND CALCULATION

To test the SAS2 on natural snowpacks, 10 field sites were selected in the Canadian Rocky Mountains, Alberta, Canada (Table I). Because of a wide range of vegetation covers, slope, wind exposure, solar irradiance, precipitation, elevation and microscale topography, snowpacks develop in the mountains with large variability in depth, density, temperature, and wetness. These environmental factors provided a number of ideal locations for testing the SAS2 system during the winter and spring of 2012. The maximum snow depth at all of these sites was ~2 m.

At the UCS (Upper Clearing Stationary) site in Marmot Creek Research Basin, a stationary version of the SAS2 was deployed on a boom arm suspended over the snowpack surface for the whole winter and spring during which a snowpack accumulated and ablated (Figure 2d). Small evergreen trees were present at this site under the snow surface. The site was part of a comprehensive snowpack mass and energy balance measuring system. A Campbell Scientific SR50 ultrasonic snow depth sensor was placed next to the SAS2 outside of the footprint of the SAS2 acoustic wave. The SR50 was used to record the height of snow (hereafter HS) corresponding to the snow depth. A narrow-view thermal infrared (IR) thermometer was used to determine surface temperature and a type-E thermocouple array ('snowharp') developed by Helgason and Pomeroy (2012) was located under the snow surface to characterize the thermal structure of the snowpack (Figure 2e).

The snowharp array was used for comparison with acoustic measurements by averaging the thermocouple measurements only over the depth of the snowpack. The snow depth at the stationary site was measured using the SR50 and only the temperature output from thermocouples that were covered with snow were used to compute the average snowpack temperature. The SR50 snow depth measurements were also used to select as maximum cutoff depth for signal analysis (Section Inverse Model).

Because of power consumption of the SAS2 (~2 amps max), the SAS2 was programmed to turn itself on and take an acoustic snow sample once every hour. All other devices were sampled by a Campbell Scientific (Logan, Utah, USA)

Table I. Names, acronyms, and geographic locations of field sites. Descriptive statistics of snow depth HS measured using a snow depth rod

#	Name	Acronym	Latitude (°N)	Longitude (°W)	Dates (2012)	Mean HS (cm)	Median HS (cm)	Min HS (cm)	Max HS (cm)	Range HS (cm)
1	Upper Clearing Stationary	UCS	50.96	115.18	1 Feb to 31 May	56	53	0	100	100
2	Boulton Campground	BC	50.64	115.11	13 March	97	100	59	110	51
3	Bow Summit	BS	51.72	116.50	14 March	175	178	119	201	82
4	Upper Clearing Portable	UCP	50.96	115.16	15 March	78	75	26	123	97
5	Sawmill Creek	SC	50.75	115.25	1 May	98	97	18	160	142
6	Bow Meadow	BM	51.70	116.48	3 May	125	125	65	162	97
7	Bow Lake	BL	51.67	116.45	3 May	58	53	51	70	19
8	Nakiska Ski Hills	NSH	50.94	115.15	4 May	49	44	3	1.6	113
9	Black Prince Cirque	BPC	50.70	115.20	4 May	57	56	22	92	70
10	Icefields Parkway Forest Site	IPFS	51.72	116.49	1 June	43	42	30	55	25

datalogger once every minute and averaged to store values on a 15-min interval. Snowpits were dug next to the stationary SAS2 device to measure snow density using a Snowmetrics (Fort Collins, Colorado, USA) triangular gravimetric sampler (Granberg and Kingsbury, 1984) and a Sartorius electronic balance; liquid water content with a Denoth dielectric meter (Denoth, 1989, 1994); and snowpack temperature with a calibrated dial thermometer typically used in snowpack measurement kits for avalanche hazard assessment (Figure 2f). Samples were taken every 10 cm of depth and individual snow strata were sampled. The samples were converted to equivalent depth-averaged values.

The portable version of the SAS2 (Figure 2c) was taken to the field sites listed in Table I in late winter and spring of 2012 and deployed using the child carrier. The chariot carrier was pushed along a transect and held still during each measurement. Immediately after each acoustic sample was taken with the portable version of the SAS2, snow depth was measured using a rod and bulk snow density was determined using an ESC30 (Farnes *et al.*, 1980, 1982) snow sampling tube and weigh scale. The rod-based measurements of snow depth were used to select a maximum cutoff depth for signal analysis (Section Inverse Model).

RESULTS

Comparison of observations

Observations were compared using Root Mean Squared Difference (RMSD) and Mean Bias (MB) (Fang *et al.*, 2010). Because of the range of RMSD and MB values at all of the field sites, some comparisons were made not only between acoustic and gravimetric techniques, but also between two gravimetric sampling techniques (snowtube and snowpit, Section SWE and Density Measurements). These comparisons help to define a range of RMSD and MB that is acceptable within the context of this study.

Ultrasonic and SAS2 measurements

The SR50 is an ultrasonic pulse-based measurement system that operates on principles similar to monopulse sonar and radar systems (Goodison *et al.*, 1988). Because the duration of the SR50 pulse is in the millisecond time range, the time-integrated energy of the sound wave produced by the SR50 is less than the time-integrated energy of the MLS sound wave sent from the SAS2 suspended over the surface of the snowpack. Unlike the SR50 (Figure 3a), time series of parameters measured by the SAS2 (Figures 3b, d and 5a, d) do not show spurious measurement spikes of large magnitude, indicating the robustness of the continuous-wave MLS signal with respect to external noise, relative to pulse-based measurement systems. Moreover, unlike the ultrasonic SR50 sound waves that are reflected from the snow surface, the audible sound wave produced by the SAS2 will penetrate the snowpack.

SWE and density measurements

At the UCS site, the RMSD between stationary SAS2 and snowpit stratified gravimetric measurements indicated

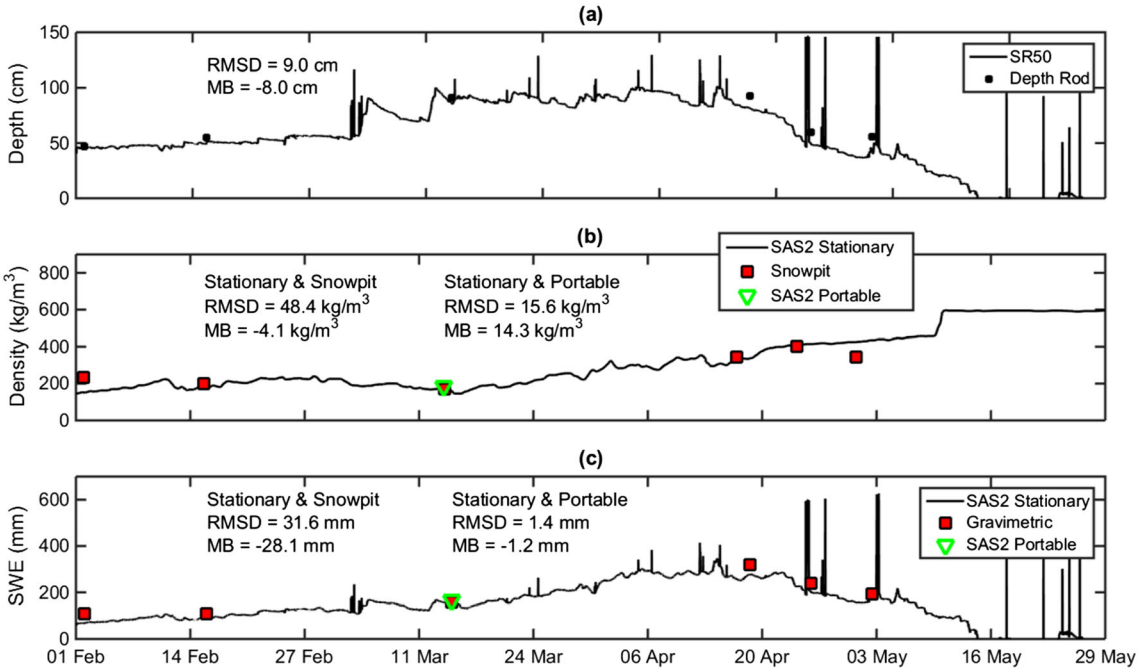

Figure 3. Upper Clearing Stationary (UCS) site time-series data showing (a) SR50 snow depth HS, (b) average density $\overline{\rho}$, and (c) snow water equivalent (SWE). SAS2, **S**ystem for **A**coustic **S**ensing of **S**now; RMSD, Root Mean Squared Difference; MB, Mean Bias

that the SAS2 under-predicted the gravimetric snowpack density measurements (Figure 3b). The RMSD value was the same order of magnitude as the RMSD values determined by comparing gravimetric and acoustic samples of snow density collected using the portable version of the SAS2 (Table III). SWE values at the UCS site were under-predicted as well (Figure 3c). This is not surprising because SWE is the numerical product of snow depth and density and the SR50 used to measure HS at the UCS site also underpredicted when compared to manual observations of depth. Figure 3b shows that a general densification of the snowpack was apparent over the observation season because of snowpack metamorphism and compaction.

Although some variation in results can be explained by hardware differences between the stationary and portable versions of the SAS2, an observation made on 15 March by the portable version of the SAS2 situated close (~2 m) to the stationary version of the SAS2 suggests that the stationary and portable versions of the acoustic gauge can obtain similar measurement results, as suggested by the low RMSD and MB values that are used to compare the measurements (Figure 3).

On 12 May, the acoustic snow density rose to 595 $kg\,m^{-3}$ and remained at this density until the end of the observation season. The snow depth measured by the SR50 was 12.8 cm on 12 May, and all snow had ablated by 14 May. Despite a small drop in the acoustic measurement of density to 592 $kg\,m^{-3}$ on 23 May when ~5.8 cm of snowfall occurred, the nearly constant acoustic snow density may represent a limitation of the acoustic method to measure wet, old-season snow that had undergone extensive metamorphism over the snow accumulation and ablation season. Moreover, multiple reflections between the ground surface and the top layer of the snowpack (Section Acoustic Imaging Examples) may have been a limiting factor in the determination of snow density at this time.

Figure 4 and Tables II and III show the RMSD and MB between ESC30 snowtube, snowpit stratified gravimetric, and SAS2 acoustic measurements of density and SWE. The small MB between these quantities (Table II) indicated that although the acoustic-determined density was slightly under-predicted, the SAS2 was able to obtain more accurate measurements than the ESC30 snowtube, relative to comparisons made between ESC30 snowtube and gravimetric snowpit measurements. The SAS2 can therefore be used as a replacement technology for non-invasively determining depth-averaged density in lieu of a snowtube. The RMSD between ESC30 snowtube measurements of SWE and acoustic measurements of SWE showed slight over-prediction of SWE. The maximum snow depth observed at all of the 10 observation sites was 2 m. This indicated that the SAS2 system was able to obtain acoustic samples of snow for snow at least 2 m in depth.

Table III aggregates data comparisons for all of the sites, showing that the RMSD magnitudes for site comparisons between snowpit and acoustic measurements of density were less than the RMSD values between snowpit and ES30 snowtube density. The limitations of evaluating the portable SAS2 against the ESC30 are that the ESC30 was less accurate than the SAS2 when compared to stratified gravimetric sampling from snowpits and so should not necessarily be considered a 'true density.' However, there is value in evaluating SAS2 performance at a wide range of sites and environmental conditions, and no other instrument could provide rapid estimation of density for comparison purposes. The Boulton Campground (BC) site data was collected early in the melt period. Acoustic observations of snow density collected at the Bow Summit (BS) site had lower RMSD and MB magnitudes when compared to the ESC30 densities than those at the BC site; this is likely because of smaller amounts of buried vegetation at the BS site leading to smaller acoustic scattering of the sound waves in snow. The Upper Clearing Portable (UCP) site data points showed more scatter than the previous BC and BS sites (Figure 4) and a higher range of acoustic densities (Table III) because of error introduced by acoustic scattering caused by buried vegetation (small trees) in the clearing and in the forest. The ESC30 tube must avoid buried vegetation when sampling a snow core; snow surveyors typically resampled until a vegetation-free core was obtained. However, the SAS2 has a larger sampling footprint than the ESC30 and will still attempt a measurement from snow mixed with buried vegetation.

The Sawmill Creek (SC) site data, collected later in the snow season, had higher densities than the previous sites because of snowpack metamorphism and higher levels of liquid water content (Table VI). The acoustic densities at the SC site showed greater error than the UCP and BS sites because of refraction of sound in the vicinity of tree wells, scattering of sound by buried vegetation in a clearing and forest, as well as possible scattering and mode conversion of sound waves because of the presence of liquid water in the pore spaces of the snowpack. Compared to all of the sites in Table III, the Bow Meadow (BM) site had the lowest RMSD values because of snowpacks with small amounts of buried vegetation that reduced acoustic scattering as well as snowpack stratigraphy with layer boundaries that best approximated horizontal lines.

The Bow Lake (BL) site dataset – collected on snow that had accumulated on the ice of a frozen lake – exhibited the highest error between gravimetric and acoustic measurements of snow density, possibly because of acoustic scattering and mode conversion of sound waves by ponded water on top of the lake ice—this water completely filled the pore spaces of the snow and increased the scatter in the data points collected at this site (Figure 4). The mean liquid water content determined

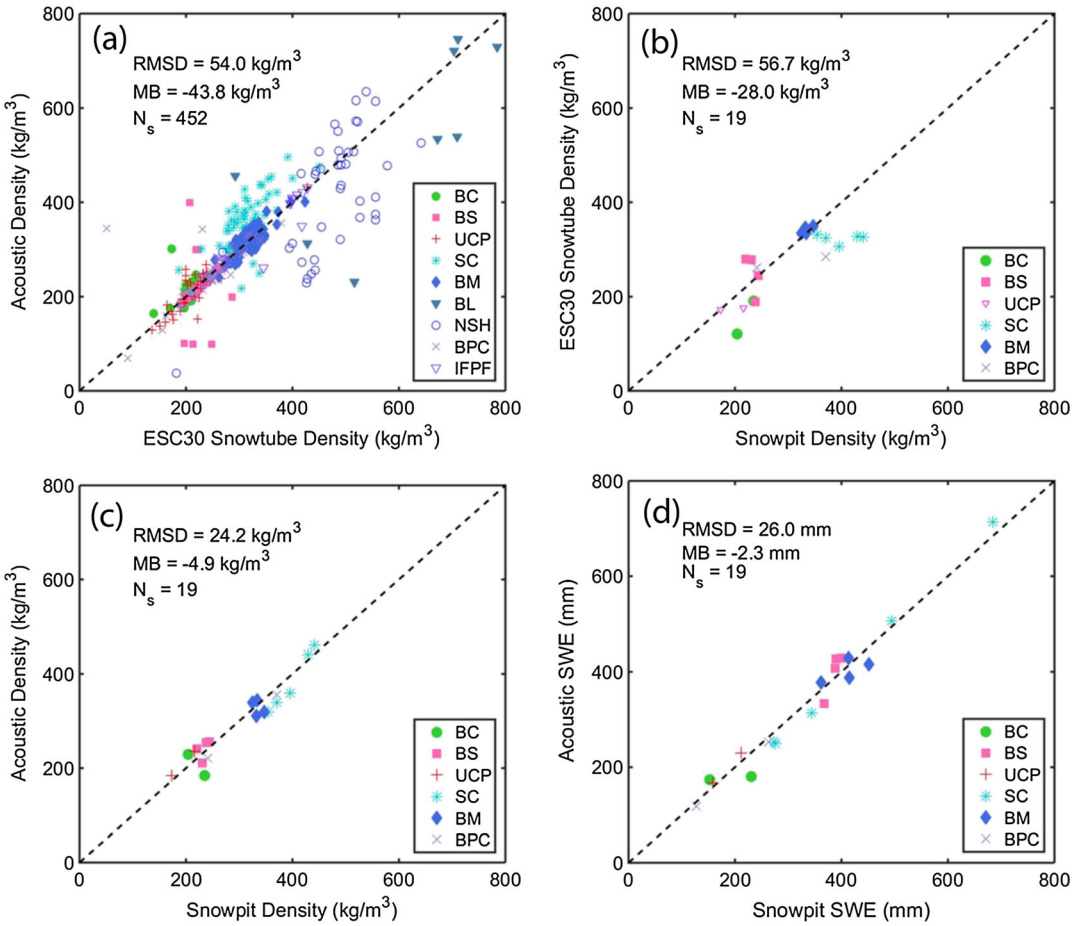

Figure 4. (a) Comparison between depth-averaged density measured using an ESC30 snow tube and depth-averaged acoustic density measured using the portable version of the **S**ystem for **A**coustic **S**ensing of **S**now (SAS2). (b) Comparison between depth-averaged snowpit density and average density measured using an ESC30 snow tube. (c) Comparison between depth-averaged gravimetric snowpit density and depth-averaged acoustic density measured using the portable version of the SAS2. (d) Comparison between SWE measured using a snowpit and SWE measured using the portable version of the SAS2. The dashed black line on the plot is the 1 : 1 line. The Boulton Campground (BC), Bow Summit (BS), Upper Clearing Portable (UCP), Sawmill Creek (SC), Bow Meadows (BM), Bow Lake (BL), Nakiska Ski Hills (NSH), Black Prince Cirque (BPC), and Icefields Parkway Forest (IFPF) sites are listed in the legend. The number of samples is given as N_s

Table II. Overall comparisons between gravimetric and acoustic measurements of density $\overline{\rho}$ and SWE

Comparison	$\overline{\rho}$ RMSD (kg m^{-3})	$\overline{\rho}$ MB (kg m^{-3})	SWE RMSD (mm)	SWE MB (mm)	N_s
ESC30 and SAS2	54.0	−43.8	47.3	9.00	452
Snowpit and ESC30	56.7	−28.0	112.4	−10.11	19
Snowpit and SAS2	24.2	−4.9	26.0	−2.30	19

The number of samples is N_s.

using acoustics at the BL site was the second-highest of all of the field sites (Table VI), with higher levels of liquid water content only observed at the Icefields Parkway Forest (IFPF) site in the month of June.

Artificial, groomed snow at the Nakiska Ski Hill (NSH) site showed an under-prediction of snow density by the SAS2 but a higher accuracy than the BL site (Table III) because of a lack of ponded water. The BPC site transect data, collected on same day as the NSH site transect data, showed lower RMSD error than the dataset collected at the NSH site. Despite the presence of a few outliers (Figure 4a), the IFPF site sample points had a lower RMSD error than the BL or NSH dataset. This suggested that although the snowpack was observed to be very wet at this field site because of concurrent rainfall, ponding of meltwater did not occur and water did not accumulate in

Table III. Comparisons between gravimetric and acoustic measurements of density $\overline{\rho}$ at individual field sites. Observations that are not available are marked with 'NA.' The RMSD, MB, and number of samples N_s are listed. Descriptive statistics of density $\overline{\rho}$ (kg m^{-3}) measured using the SAS2. The 'NA' in the table above indicates that the comparison is 'Not Applicable' because some field measurements were not collected

Site	Dates (2012)	Mean acoustic density (kg m^{-3})	Median acoustic density (kg m^{-3})	Min acoustic density (kg m^{-3})	Max acoustic density (kg m^{-3})	Range acoustic density (kg m^{-3})	$\overline{\rho}$ comparison	RMSD (kg m^{-3})	MB (kg m^{-3})	N_s
UCS	1 February to 31 May	291	241	145	597	452	ESC30 and SAS2	NA	NA	NA
							Snowpit and snowtube	NA	NA	NA
							Snowpit and SAS2	48.4	−4.10	6
BC	13 March	202	195	154	261	107	ESC30 and SAS2	47.1	19.5	12
							Snowpit and snowtube	67.4	64.5	2
							Snowpit and SAS2	40.5	−12.5	2
BS	14 March	242	239	190	312	122	ESC30 and SAS2	29.0	3.2	117
							Snowpit and snowtube	45.0	−14.3	4
							Snowpit and SAS2	18.1	7.3	4
UCP	15 March	250	234	130	456	327	ESC30 and SAS2	25.2	3.8	35
							Snowpit and snowtube	28.0	20.4	2
							Snowpit and SAS2	15.5	15.0	2
SC	1 May	364	358	210	600	390	ESC30 and SAS2	62.3	43.5	65
							Snowpit and snowtube	82.6	75.2	5
							Snowpit and SAS2	27.7	−14.0	5
BM	3 May	317	320	240	401	161	ESC30 and SAS2	17.9	−2.8	63
							Snowpit and ESC30	19.9	−5.5	4
							Snowpit and SAS2	8.2	−6.2	4
BL	3 May	534	537	231	745	514	ESC30 and SAS2	147.4	−68.9	8
							Snowpit and ESC30	NA	NA	NA
							Snowpit and SAS2	NA	NA	NA
NSH	4 May	420	459	38	635	597	ESC30 and SAS2	109.5	−53.5	40
							Snowpit and ESC30	NA	NA	NA
							Snowpit and SAS2	NA	NA	NA
BPC	4 May	258	255	69	394	325	ESC30 and SAS2	50.1	7.3	45
							Snowpit and ESC30	62.6	33.7	2
							Snowpit and SAS2	18.2	−18.0	2
IFPF	1 June	374	405	260	431	171	ESC30 and SAS2	36.7	−13.5	9
							Snowpit and ESC30	NA	NA	NA
							Snowpit and SAS2	NA	NA	NA

the pore spaces of the snowpack. Because the snowpack was well-drained at the IFPF site, this reduced acoustic scattering and mode conversion occurring because of the ponded water. This reduced scatter in the data points. It should also be noted that on-board signal processing was demonstrated within the SAS2 at the IFPF site and differences between the SAS2 and ESC30 densities were not larger than when post-processing was used for other sites.

Thermal measurements

For most of the observation period, the snowharp and depth-averaged snowharp temperature observations at the UCS site (Figure 5a–c) show results that are physically reasonable. Although the differences between observations have an error within a few degrees Celsius, the results are encouraging because the order of magnitude of the acoustic measurements is the same as the measurements made by thermocouples. Further research is required to improve the acoustic model and improve the accuracy of acoustic observations of snow temperature.

However, exposed and shallowly buried thermocouples suspended on the snowharp wires will heat in the sun, and this adds another source of experimental error when attempting to make comparisons between acoustic and thermocouple measurements of temperature. For comparison purposes, the snowharp measurements were constrained to ≤0 °C, allowing for comparison with the acoustic SAS2 measurements that were constrained to ≤0 °C by the UTAM model. Over the entire period of observation, the UTAM model gave estimates of snow temperature that were no greater than 0.6 °C above the melting point of snow at 0 °C. When snow was present on the ground during the observation period, only 98 acoustic samples of snow had to be constrained to ≤0 °C. This constraint was applied to make the SAS2 observations physically reasonable. The model predicted temperatures slightly greater than 0 °C because of the influence of temperature gradients above the snowpack that caused the SAS2 measured air temperature to differ from the actual air temperature near the snow surface. There is a need for further experimentation to characterize the influence of these temperature gradients on acoustic sensing of snow.

The SR50 ultrasonic snow depth measurements are also shown on Figure 5b, indicating that there are four periods of observation. The averaged snowharp temperatures (Figure 5a) only use thermocouples that are

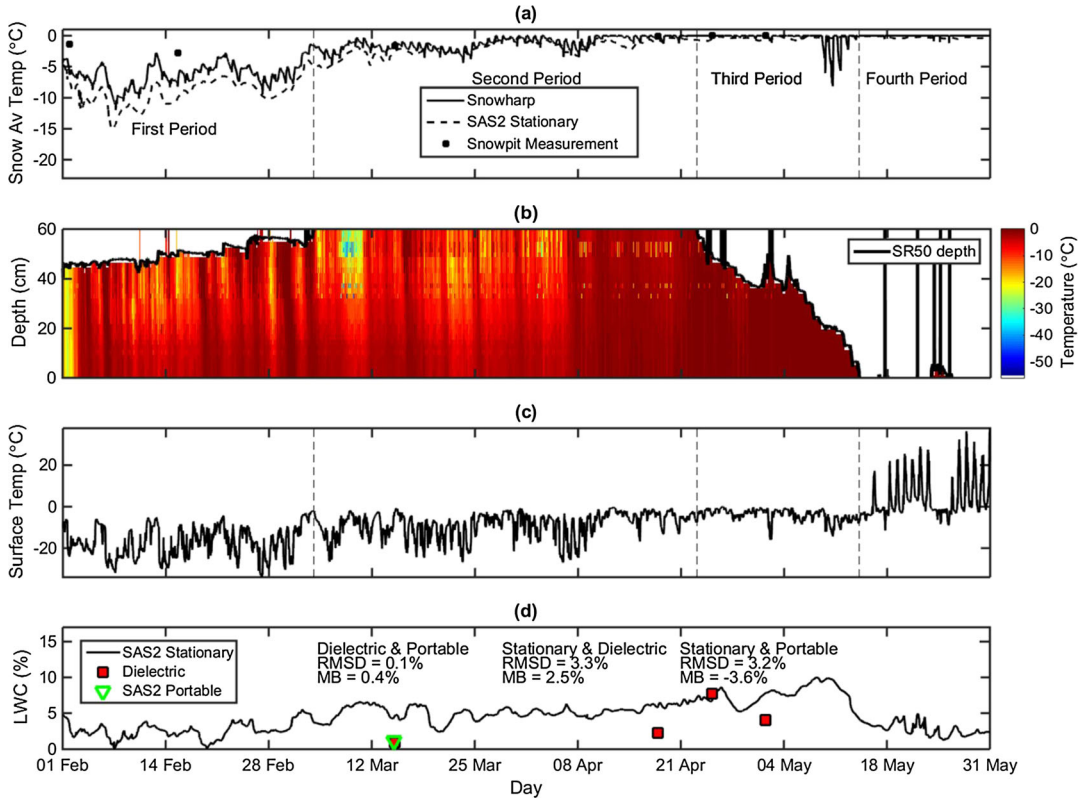

Figure 5. Upper Clearing Stationary (UCS) site time-series data showing (a) depth-averaged snowharp temperature and depth-averaged acoustic temperature, (b) spatial distribution of temperature observed using the snowharp, (c) surface temperature measured using the infrared thermometer, and (d) liquid water content (LWC) θ_w as LWC. SAS2, **S**ystem for **A**coustic **S**ensing of **S**now; RMSD, Root Mean Squared Difference; MB, Mean Bias

completely covered by snow. These are the thermocouples situated at distances from the ground less than the snow depth measured by the SR50.

The first period coincided with the beginning of the observation season when the snowharp was not completely covered by snow; the second period coincided with the time when the snowharp was completely covered by snow; the third period coincided with the time of ablation, when there was a reduction in snow depth and uneven snow topography around the snowharp; and the fourth period coincided with the time when most of the snow had ablated. The RMSD and MB between snowharp and SAS2 measurements for each period are given by Table IV. Because comparisons between observations are only made with thermocouples that are completely covered with snow, the fourth period provides an estimate of the UTAM model performance for snow of small vertical depth (low HS).

The RMSD between snowharp and SAS2 measurements were highest during the first period of observation, Feb to early March, compared to the second, third, and fourth observation periods, early March to mid-May. Cold weather and solar heating of the uppermost thermocouples in the snowpack contributed to over-measurement of upper layer temperatures by the snowharp in the first period. A second important consideration in reviewing these measurements is that snowpit observations were stratified and so sampled equally from all depths, but snowharp measurements are restricted to the ground surface to 60 cm above the ground and so preferentially sampled the middle and lower snowpack in the second period when snow depths approached 1 m. The RMSD and MB magnitudes were lower during the second period of observation, and by the third period when snow ablation was occurring, the snow temperature was often close to 0 °C. Because both the snowharp and acoustic measurements were constrained to ≤ 0 °C, both the RMSD and MB magnitudes remained low during the third period of rapid ablation as solar heating of thermocouples above 0 °C would not be evident in the snowharp data. Though the RMSD remained low, the MB magnitude during the fourth period, when the snowpack was intermittent, was higher than the other periods of observation.

Over the entire observation period (Table IV) the snowharp and acoustic measurements had the lowest RMSD and MB magnitudes. The snowpit and acoustic measurements had the highest RMSD and MB magnitudes—this may have been because of spatial differences in snow temperature between the snowpit and SAS2 sampling locations. The snowpit and snowharp RMSD and MB showed values that were intermediate between the RMSD and MB values used to compare the other measurements.

Comparisons were made by temperatures measured in snowpits using a thermometer and acoustic snow temperatures measured using the portable version of the SAS2 (Table V, Figure 6). The RMSD and MB suggest that the SAS2 was able to measure snow temperature well at certain times and with substantial error at other times and that larger errors may have been associated with buried vegetation in the snowpack. Snow temperature measured by the SAS2 increased over the winter season, with higher mean temperatures apparent at the BM, BL, and NSH sites.

Figure 6 shows that acoustic and manual measurements are better correlated for temperatures below −2 °C, thereby demonstrating the errors associated with manual measurement of snow temperature by a dial-type thermometer inserted into a snowpit wall. Because the SAS2 was used to determine snow temperature before the digging of a snowpit, the acoustic measurement was non-invasive. Changes in snowpack temperature could have occurred after the snowpit was created. Moreover, an increase in error associated with the UTAM may occur at snow temperatures approaching 0 °C.

Liquid water content measurements

Over the entire period of observation at the UCS site, the stationary SAS2 and snowpit-based dielectric measurements of liquid water content indicated that dielectric measurements were under-predicted with respect to acoustic measurements (Figure 5d). Spatial differences in liquid water content between measurement locations were apparent. The dielectric liquid water content compared to the liquid water content measured by the portable version of the SAS2 demonstrated the

Table IV. Comparison of differences between snowharp and SAS2 measurements of snowpack temperature over the entire observation period at the UCS site

Measurement	First period	Second period	Third period	Fourth period	Snowpit and acoustic	Snowpit and snowharp	Snowharp and acoustic
RMSD (°C)	3.0	1.1	1.2	0.32	3.9	2.6	1.8
MB (°C)	−2.9	−0.76	−0.051	−0.27	−2.6	1.4	−1.1

Table V. Comparisons between snowpit and acoustic measurements of snowpack averaged temperature $\overline{T}$. Descriptive statistics of temperature $\overline{T}$ measured using the SAS2. The number of samples is N_s. The 'NA' in the table above indicates that the comparison is 'Not Applicable' because some field measurements were not collected

Site	Dates (2012)	$\overline{T}$ RMSD (°C)	$\overline{T}$ MB (°C)	Acoustic mean (°C)	Acoustic median (°C)	Acoustic min (°C)	Acoustic max (°C)	Acoustic range (°C)	N_s
UCS	1 Feb to 31 May	3.9	−2.6	−3.4	−1.5	−15.0	0.0	15.0	6
BC	13 March	1.4	−1.4	−4.9	−4.5	−9.0	−2.0	7.0	2
BS	14 March	0.7	0.1	−6.0	−5.6	−8.6	−3.1	5.5	4
UCP	15 March	0.7	−0.4	−4.8	−5.4	−6.5	−1.0	5.3	2
SC	1 May	2.5	−2.2	−1.3	−1.0	−4.0	0.0	4.0	5
BM	3 May	1.0	−0.7	−0.9	−0.9	−2.0	−0.1	1.9	4
BL	3 May	NA	NA	−0.3	−0.3	−0.5	−0.1	0.4	NA
NSH	4 May	NA	NA	−1.4	−1.0	−4.0	−0.5	3.5	NA
BPC	4 May	0.2	−1.5	−2.5	−2.0	−5.0	−0.9	4.1	2
IFPF	1 June	NA	NA	−0.1	−0.1	−0.3	0.0	0.3	NA

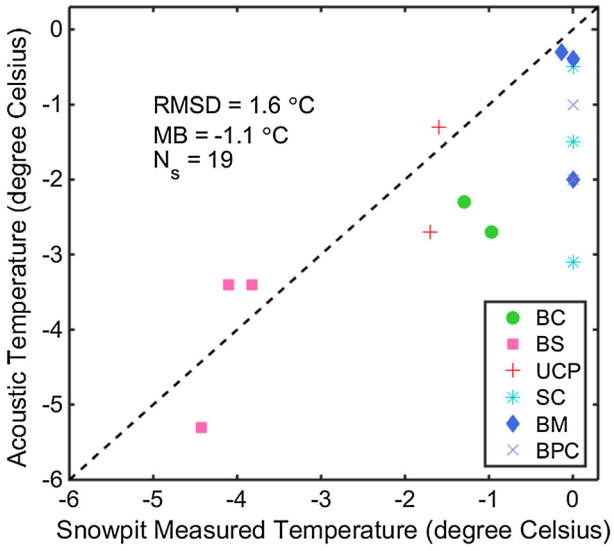

Figure 6. Comparison between depth-averaged temperature measured using snowpits and depth-averaged acoustic temperature measured using the portable and stationary versions of the **S**ystem for **A**coustic **S**ensing of **S**now at six field sites. The dashed black line on the plot is the 1 : 1 line. The Upper Clearing Portable (UCP), Upper Clearing Stationary (UCS), Boulton Campground (BC), Sawmill Creek (SC), Black Prince Cirque (BPC), Bow Summit (BS), and Bow Meadows (BM) sites are listed in the legend. The number of samples is given as N_s

ability of the SAS2 to measure $\overline{\theta}_w$ within a 0.5% RMSD difference, similar in magnitude to a ± 0.5 % liquid water content measurement error associated with individual point-based dielectric measurements (Techel and Pielmeier, 2011). Although the Techel and Pielmeier (2011) paper reports an error associated with individual point-based dielectric measurements, here we consider the SAS2 as taking individual acoustic 'samples' of snow at a given location. Although the depth-averaged liquid water content values may have errors less than 0.5%, the ± 0.5 % comparison criterion is used here in this paper to provide a threshold value for comparison.

Some observations of liquid water content $\overline{\theta}_w$ are <1.3% by volume within the dry region classified using the Techel and Pielmeier (2011) scheme, and most observations are <8% by volume as found by Kattelmann and Dozier (1999) for natural snowpacks. For wet snow during the time of ablation, the acoustic observations of liquid water content $\overline{\theta}_w$ approach 10%. This is apparent for the stationary SAS2 observations made at the UCS site as well as for measurements of liquid water content made at other field sites. The liquid water content values do not reach levels of ~0% because of the presence of irreducible water content in the snowpack resulting from the presence of a quasi-liquid layer surrounding the snow particles.

The liquid water content increased over the observation season as the snowpack warmed because of higher levels of net radiation and increasing air temperatures. This is apparent at the UCS site and at the portable sites visited later in the observation season (Figure 5d and Table VI). All observations of liquid water content made using the SAS2 are within the range of liquid water contents given by the Martinec classification scheme and the Fierz *et al.* (2009) scheme. Because the acoustic values of water content observed at the UCS site are in the same range of liquid water contents observed by other investigators, this strongly implies that the acoustic sensor measurements are physically reasonable and of similar magnitude to the findings from other researchers, although it is not possible to exactly confirm the readings.

Although the liquid water content was >3% during some periods when the snowpack had a measured depth-averaged temperature below freezing, temperatures in a near-surface layer of the snowpack may have been higher, resulting in higher levels of liquid water content as measured by the acoustic sensor. Moreover, heating of the snowpack at the snow surface, by the ground surface or by the presence of nearby vegetation may have contributed to higher levels of liquid water content at a

Table VI. Comparisons between dielectric and acoustic measurements of snowpack averaged liquid water content $\overline{\theta}_w$. The number of samples is N_s. The 'NA' in the table above indicates that the comparison is 'Not Applicable' because some field measurements were not collected

Site	Dates (2012)	$\overline{\theta}_w$ RMSD (%)	$\overline{\theta}_w$ MB (%)	Acoustic mean (%)	Acoustic median (%)	Acoustic min (%)	Acoustic max (%)	Acoustic range (%)	N_s
UCS	1 Feb to 31 May	3.3	2.5	4.2	4.1	1.0	10	9	6
BC	13 March	NA	NA	1.8	1.7	1.1	2.5	1.4	NA
BS	14 March	0.3	0.2	2.0	2.1	1.1	3.1	2.0	4
UCP	15 March	0.2	0.1	0.9	0.9	1.0	1.4	1.3	2
SC	1 May	0.8	−0.6	4.4	4.0	2.0	9.0	7.0	5
BM	3 May	0.4	0.2	3.1	3.2	1.9	4.6	2.7	4
BL	3 May	NA	NA	7.9	8.0	5.0	9.0	4.0	NA
NSH	4 May	NA	NA	6.8	7.0	4.0	9.0	5.0	NA
BPC	4 May	0.2	0.2	3.8	3.0	1.0	8.0	7.0	2
IFPF	1 June	NA	NA	8.4	8.5	7.0	9.1	2.1	NA

sampling point under the acoustic sensor. This may indicate a fundamental limitation associated with a one-layer acoustic model of snow and indicates the need for further research to develop a multi-layer acoustic model to measure snow.

Liquid water content in the snowpack is highly variable over vertical distances spanning only 50 cm (Techel and Pielmeier, 2011). Moreover, water transport through snow follows three-dimensional flow paths, with more continuity between flow fingers in a snowpack layer than flow fingers in vertically lower layers (Williams *et al.*, 2010; McGurk and Marsh, 1995).

Therefore, the measurement error between stationary and portable versions of the SAS2 may have occurred because of the presence of small-scale differences in liquid water content within the snowpack. The portable SAS2 device was used to obtain acoustic samples of liquid water content at a distance of ~2 m from the stationary device. Because of the installation of other instrumentation around the stationary SAS2 (Figure 2d), the portable SAS2 device could not be co-located with the stationary SAS2.

The error between dielectric measurements and acoustic measurements of liquid water content collected at all of the field sites was small (Figure 7 and Table VI). These results indicated that the RMSD was similar to the 0.5% measurement error associated with dielectric measurements. This demonstrated that the SAS2 was able to obtain measurements of liquid water content with the same order of magnitude as dielectric measurements.

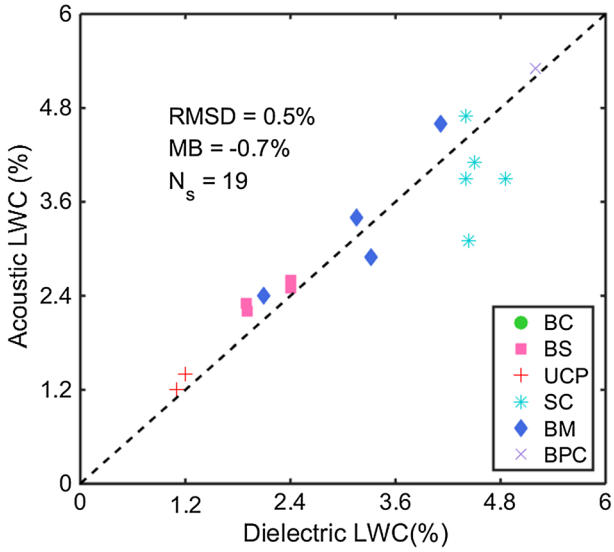

Figure 7. Comparison between depth-averaged liquid water content measured using dielectric methods and liquid water content measured using the **S**ystem for **A**coustic **S**ensing of **S**now at six field sites. The dashed black line on the plot is the 1 : 1 line. The Boulton Campground (BC), Bow Summit (BS), Upper Clearing Portable (UCP), Sawmill Creek (SC), Bow Meadows (BM), and Black Prince Cirque (BPC) sites are listed in the legend. The number of samples is given as N_s. The liquid water content is indicated as LWC.

Acoustic imaging examples

Figure 8d shows an example of an acoustic image created using the stationary version of the SAS2 at the UC stationary site on 15 March. The figure consists of processed signals arranged at offset distances using a mathematical seismic moveout operator. The elements of the image matrix have been scaled to amplitudes on the interval of [0, 1] for visual display. The observation was made on 15 March shortly before a 91-cm-deep snowpit was dug about 2 m from the acoustic sensor. Snowpack classification is given using nomenclature of the ICSSG (Fierz *et al.*, 2009). The grain size is given as E_s, and the origin of each grain is associated with the nomenclature. Classification was made by visual observations in the field by a human observer.

As shown by Figures 8a–c, the snowpit stratigraphy was comprised of a wind-crusted surface layer with clumps and hard snow (PPir, $E_s = 0.5$ mm, from 91 cm to 89 cm) overlying a layer with rounded dendrites (RGxf, $E_s = 0.5$ mm, from 89 cm to 71 cm); under this layer was a

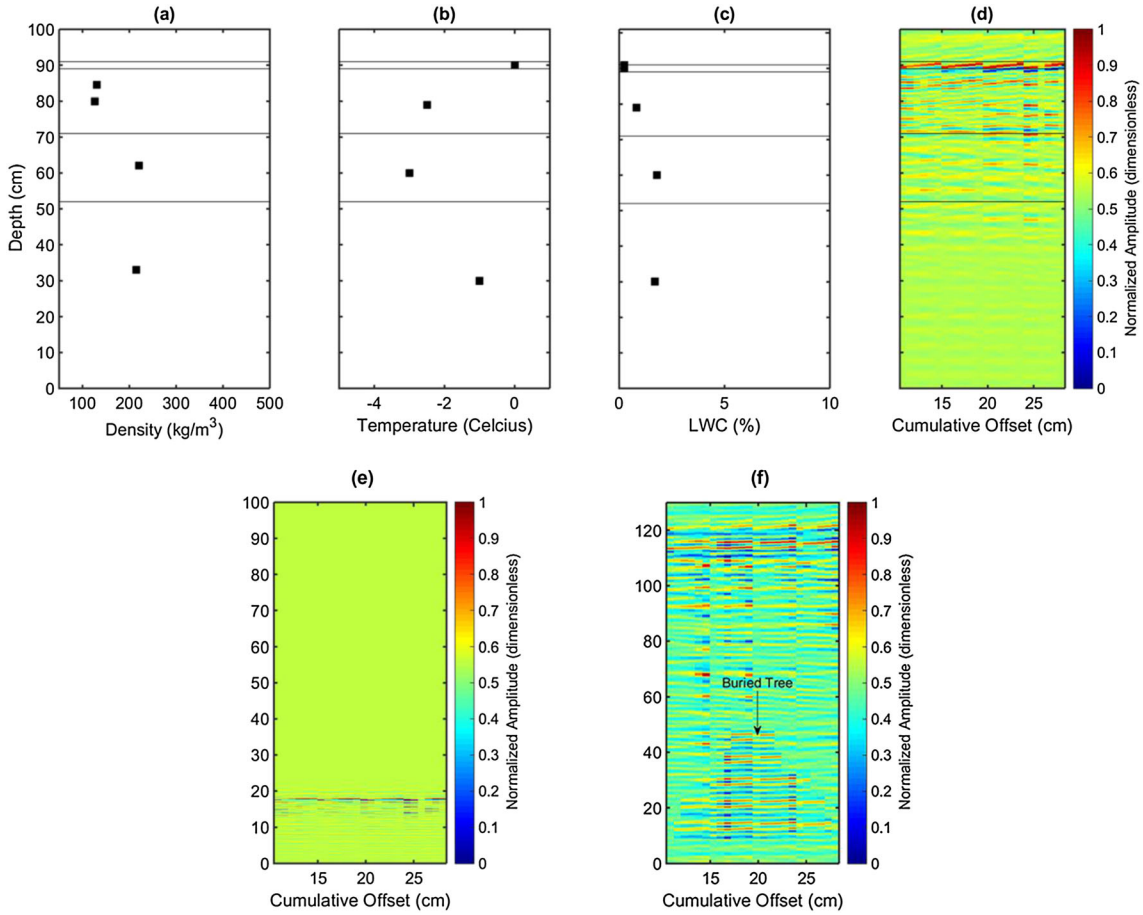

Figure 8. (a to d) Snowpit stratigraphy at Upper Clearing Stationary (UCS) site observed on 15 March at 1700 h local time. The snowpit was situated close (~2 m) to the **S**ystem for **A**coustic **S**ensing of **S**now sensor; subplots are: (a) gravimetric density measurements, (b) temperature measured from the snowpit wall using a thermometer, (c) liquid water content, and (d) acoustic image of snowpit with cumulative offset. The measurements in Figure 8(a–c) are depth-averaged over the layers indicated on the plots. Descriptions related to ISSG nomenclature are given in the text. (e) Acoustic image of snowpack at the UCS site on 12 May at 1200 h local time. (f) Image of buried conifer tree at the SC site. The location of the tree is marked on the image with an arrow. The liquid water content is indicated as LWC.

layer of rounded columnar snow crystals (MFpc, $E_s = 1$ mm, from 71 cm to 52 cm); in the lower snowpack was a layer of depth hoar composed by larger faceted crystals (DHla, $E_s = 4$ mm, from 52 cm to 0 cm). Comparisons between measurements are shown by Table VII.

The RMSD between the snowpit and acoustic measurements indicated that for this measurement, the SAS2 slightly underpredicted depth-averaged snow density. SWE was similarly underpredicted because of its reliance on density estimates. The depth-averaged snowpit temperature was slightly greater than the acoustic measurement of temperature. The RMSD between temperature measurements was within the maximum error associated with comparing two dial-type thermometers in a snowpit.

Table VII. Comparison between measurements for the example snowpit at the UCS site on 15 March 2012

Measurement	Gravimetric/ thermal/ dielectric	Acoustic	RMSD	MB
$\overline{\rho}$(kg m^{-3})	173	168	4.46	−4.46
SWE (mm)	157	142	15.6	−15.6
$\overline{T}$ (°C)	−1.60	−2.50	0.910	−0.910
$\overline{\theta}_w$	0.960	4.70	3.70	3.70

The acoustic image (Figure 8d) showed reflections from the snowpack. The resolution is qualitatively similar to a sonar image sensed using a sediment-profiling sonar system (Lurton, 2002) or a medical ultrasonography image (Ng and Swanevelder, 2011). Acoustic reflections occur because of changes in acoustic impedance, whereas an observer uses a visual interpretation of the layer boundaries. However, the acoustic images coincide quite well with the visual interpretation.

At 91 cm above the ground, the acoustic image from the SAS2 shows a high-amplitude reflection associated with the sound wave crossing the air–snow interface as it entered the snowpack. The high-amplitude reflection occurred because of differences in acoustic impedance

between air and snow. A low-amplitude reflection was visible at 89 cm above the ground after the sound wave exited the wind-crusted layer and penetrated to a greater depth beneath the snow surface. Within the second snowpack layer from 89 cm to 71 cm above the ground, acoustic scattering of the sound wave and internal reflections caused a series of linear features to appear in the image. These linear features disappear below 71 cm above the ground, indicating the start of another layer in the snowpack. The linear features are of higher amplitude than the features in the preceding layer from 71 cm to 52 cm above the ground. From 52 cm above to the ground surface, there was a loss of resolution and an increase in attenuation as the sound wave propagated into the depth hoar layer; this increased attenuation occurred as the sound wave propagated through a porous medium comprised of coarse particles.

There is a need for additional research to quantify the effects of the ground on the propagation of the acoustic wave. In many observations made with the SAS2 system, excessive attenuation near the bottom of the snowpack associated with the presence of depth hoar did not permit for the ground interface to be clearly demarcated and an effective signal cutoff time was utilized in lieu of identification of the ground surface from the acoustic image.

On 12 May, shortly after the acoustic measurements of density reached a constant value, the snowpack depth at the UCS site was 12.8 cm, but the corresponding acoustic image (Figure 8e) showed the interface at the surface of the snowpack as being slightly higher (near 18 cm) because of differences in snow surface topography and additional spurious reflections from the snowpack. The surface of the snowpack was very wet, and the reflection of sound energy from the snow surface was high. Because of the presence of ponded water beneath the snow surface, excessive attenuation of the sound wave occurred at distances close to the ground surface.

Excessive attenuation near the bottom of the snowpack may also reduce the possibility of detecting buried vegetation. Although small coniferous trees were buried under the snowpack at the UCS location, these are not shown by the acoustic images, and this suggests that the geometric shape and size of the vegetation may affect the ability for acoustic detection of buried objects. This is demonstrated by an acoustic observation made by the portable version of the SAS2 at the SC site (Figure 8f, Table VIII), where a buried conifer tree with a maximum crown diameter of ~60 cm was detected by the SAS2. The top of the tree is clearly visible in the image, yet some of the branches were not detected. Acoustic scattering of sound waves by the tree is clearly visible in the acoustic image at distances above the tree within the snowpack from 60 cm to 120 cm. A layer of fresh snow and an acoustic impedance discontinuity at the air–snow interface is visible at the surface of the snowpack (120 cm). The RMSD and MB corresponding to the acoustic observation of this image (Table VIII) show that the acoustic and gravimetric measurements remain within the same order of magnitude of other measurements made at the SC site (Table III), but are slightly higher because of errors introduced by acoustic scattering. Additional research involving mathematical modelling and acoustic snow measurements is thereby required to fully quantify the effects of buried vegetation on the propagation of acoustic waves in snow.

Table VIII. Comparison between measurements corresponding to the image of the buried conifer (Figure 8f). The 'NA' in the table above indicates that the comparison is 'Not Applicable' because some field measurements were not collected

Measurement	SR50 gravimetric	Acoustic	RMSD	MB
$\overline{\rho}$(kg m^{-3})	392	496	104	104
SWE (mm)	470	595	125	125
$\overline{T}$(°C)	NA	−2.3	NA	NA
$\overline{\theta}_w$ (%)	NA	1.8	NA	NA

Semi-infinite medium sensitivity analysis

To assess the effect of signal cutoff time on the error associated with measuring snowpack variables using the SAS2 and the inverse UTAM model, an error analysis was performed using acoustic data collected at all of the field sites with the stationary and portable versions of the SAS2 (Figure 9).

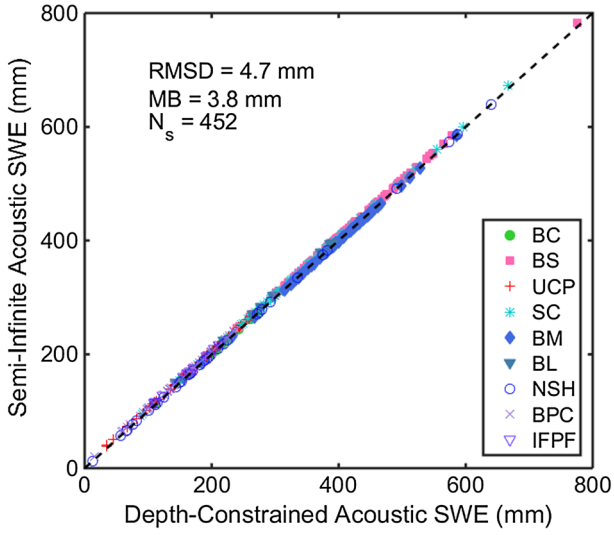

Figure 9. Comparison between depth-constrained acoustic measurements of snow water equivalent (SWE) and acoustic measurements of SWE with a signal cutoff time of 1.6 s (semi-infinite acoustic SWE). The dashed black line on the plot is the 1 : 1 line. The number of samples is given as N_s

The semi-infinite snowpack medium is defined here as a medium where the maximum signal cutoff time is associated with an equivalent depth that may be orders of magnitude larger than the actual snow depth. This allows for the model to be tested for errors associated with not measuring snow depth.

The error analysis was conducted by increasing the signal cutoff time up to 1.6 s, which is the duration of the MLS source signal. Over all of the outputs of the UTAM model and for all sampling points, this increased the average error by only 3.28%. Figure 9 shows the RMSD and MB between acoustic measurements of SWE with a cutoff time set by depth-rod measured snow depth (depth-constrained) and acoustic measurements of SWE with a signal cutoff time of 1.6 s (semi-infinite).

The insensitivity of the inverse UTAM model to the cutoff time is because of reflections of relatively low amplitude that occurred at times after the sound wave propagated through the snowpack. Attenuation of the sound wave in snow near the bottom of the snowpack is assumed to have occurred because of the presence of depth hoar. Late-time reflections therefore contributed relatively little error to the inputs of the inverse UTAM model. These results suggest that the SAS2 can be used for SWE estimation where no snow depth information can be collected for assimilation into the UTAM model.

CONCLUSIONS

This paper reported the first tests of the SAS2 as an electronic sensing system designed to non-invasively measure snow density, liquid water content, and temperature using acoustics. The SAS2 was tested at 10 field sites in the Canadian Rockies. A modified version of the Biot-Stoll equations (UTAM) was used to obtain these measurements.

The SAS2 is a modified and updated version of previous acoustic sensing devices that have been created, deployed and tested. Unlike these previous devices, the SAS2 presented in this paper utilizes more than one microphone situated at an offset distance to a loudspeaker. This paper thereby serves as an update showing the development of an acoustic sensing method.

Comparisons between stratigraphic snow profile and snowtube bulk gravimetric measurements of snow density were less accurate than comparisons between snowpit stratified gravimetric and SAS2 acoustic measurements (Table II and Section SWE and Density Measurements), suggesting that the SAS2 has an accuracy comparable to snowpit measurements of density and could be used in lieu of digging a snowpit. The ESC30 snowtube was not as accurate as SAS2 and snowpit measurements when measuring SWE and snow density and so the portable and stationary SAS2 could be used as a replacement technology for a snowtube for operational snow surveys of SWE and monitoring purposes at a meteorological station. Tests show that while SAS2 performance is enhanced by assimilation of independent snow depth measurements used to select a cutoff time for signal processing (Section Inverse Model), perfectly adequate SWE estimations are possible from sound waves alone (Section Semi-Infinite Medium Sensitivity Analysis). It should be noted that, unlike gravimetric sampling, the SAS2 can operate when there is buried vegetation such as small evergreen trees, though its accuracy likely drops in these circumstances as the buried objects interfere with the sound signal. There is a need for further research to model and measure the interactions between sound waves and buried vegetation in snow.

SAS2 measurements of liquid water content were similar and within a nominal 0.5% threshold error associated with dielectric measurements. This indicated that the SAS2 was able to estimate similar liquid water contents to a dielectric device. Acoustic measurements of snow temperature sometimes had greater errors than snow temperature measurements made using thermometers and thermocouples but the advantage of being non-invasive and non-destructive.

The focus of this paper is on testing of the device, indicating that the SAS2 can provide non-invasive, non-destructive measurements of snowpack physical properties. Future work is required to optimize system design and provide further insight into processes of acoustic scattering and mode conversion during sound wave propagation through snow. This may provide insight into development of a well-posed inverse model that is able to obtain layered estimates of snowpack properties in lieu of the equivalent one-layer model utilized in this paper. Modelling could also be used to gain insight into the maximum depth, density and wetness of snow that can be sensed by the SAS2. The maximum snow depth over which acoustic measurements were made was ~2 m, densities did not exceed ~800 $\mathrm{kg\,m^{-3}}$ and liquid water content did not exceed ~5% and so performance of the device outside of this range is currently unknown.

The SAS2 shows great promise for a number of potential applications in snow hydrology. For continuous monitoring of snow, variables measured by the SAS2 could be used as internal state variables in mathematical models of snowpack evolution. Rather than estimating internal state variables of the snowpack from mass and energy fluxes, the acoustic estimates could be assimilated directly into snowpack models. This suggests the way forward for a new generation of snowpack evolution models that are not driven by mass and energy fluxes at snowpack boundaries. However, a multi-layer acoustic model of snow would also be beneficial to use along with

new multi-layer snow evolution models, and further research is required to achieve this goal.

There is a need to validate, test, and deploy a network of SAS2 gauges at a number of field sites situated at different locations so that the models and instrumentation described in this paper can be verified, additionally tested in a number of cold environments, and potentially improved.

ACKNOWLEDGEMENTS

We would like to thank the National Sciences and Engineering Research Council of Canada (NSERC) through its Discovery, Research Tools, and Instruments and Canada Graduate Scholarships programmes, Alberta Environment and Sustainable Resource Development, and the U of S Global Institute for Water Security for funding this research. Field assistance from May Guan, Xing Fang, Daniel Gunther, Charles Maule, Mike Demuth, and Chris Marsh is gratefully acknowledged. The Department of Electrical and Computer Engineering at the University of Saskatchewan is to be thanked for providing access to an anechoic chamber for acoustic measurements. We thank the editors and reviewers whose comments have greatly improved this paper.

REFERENCES

Albert DG. 1993. Attenuation of outdoor sound propagation levels by a snow cover. CRREL Report 93-20, Cold Regions Research and Engineering Laboratory: Hanover, New Hampshire.

Anderson JD. 1991. *Fundamentals of Aerodynamics*. McGraw-Hill: New York.

Barger JE. 1998. Sonar systems. In *Handbook of Acoustics*. John Wiley & Sons: New York; 435–455.

Barnett TP, Adam JC, Lettenmaier DP. 2005. Potential impacts of a warming climate on water availability in snow-dominated regions. *Nature* **438**(7066): 303–309. DOI:10.1038/nature04141.

Bartelt P, Lehning M. 2002. A physical SNOWPACK model for the Swiss avalanche warning Part I: numerical model. *Cold Regions Science and Technology* **35**: 123–145.

Bartlett PA, MacKay MD, Verseghy DL. 2006. Modified Snow Algorithms in the Canadian Land Surface Scheme: Model Runs and Sensitivity Analysis at Three Boreal Forest Stands. *Atmosphere-Ocean* **44**: 207–222.

Berryman JG. 1980. Confirmation of Biot's theory. *Applied Physics Letters* **37**: 382–384.

Bilaniuk N, Wong GSK. 1993. Speed of sound in pure water as a function of temperature. *Journal of the Acoustical Society of America* **93**(3): 1609–1612.

Bilaniuk N, Wong GSK. 1996. Erratum: Speed of sound in pure water as a function of temperature. *Journal of the Acoustical Society of America* **99**(5): 3257.

Borish J, Angell JB. 1983. An efficient algorithm for measuring the impulse response using pseudorandom noise. *Journal of the Audio Engineering Society* **31**: 478–487.

de Bruin CGM, Wapenaar CPA, Berkhout AJ. 1990. Angle-dependent reflectivity by means of prestack migration. *Geophysics* **55**(9): 1223–1234. DOI:10.1190/1.1442938.

Carrion PM, VerWest B. 1987. A procedure for inverting seismic data to obtain Q-profiles. *Inverse Problems* **3**: 65–71.

Chavent G. 2009. *Nonlinear Least Squares for Inverse Problems: Theoretical Foundations and Step-by-Step Guide for Applications*. Springer: Dordrecht, Heidelberg, London; New York.

Claerbout JF. 1992. *Earth Soundings Analysis: Processing Versus Inversion*. Blackwell Scientific Publications: Boston.

Colbeck SC. 1972. A theory of water percolation in snow. *Journal of Glaciology* **11**: 369–385.

Colbeck SC. 1974a. The capillary effects of water percolation in homogeneous snow. *Journal of Glaciology* **13**: 85–97.

Colbeck SC. 1974b. Water flow through snow overlying an impermeable boundary. *Water Resources Research* **10**: 119–123.

Colbeck SC. 1975. A theory for water flow through a layered snowpack. *Water Resources Research* **11**: 261–266.

Colbeck SC. 1977. Short-term forecasting of water run-off from snow and ice. *Journal of Glaciology* **19**: 571–588.

Colbeck SC. 1982. An overview of seasonal snow metamorphism. *Reviews of Geophysics and Space Physics* **20**(1): 45–61.

Colbeck SC. 1997. A review of sintering in seasonal snow. CRREL Report 97-10, Cold Regions Research and Engineering Laboratory: Hanover, New Hampshire.

Cox H. 1989. Fundamentals of bistatic active sonar. In *Underwater Acoustic Data Processing*. Springer: Dordrecht, Boston, London; 3–24.

Denoth A. 1989. Snow dielectric measurements. *Advances in Space Research* **9**: 233–243.

Denoth A. 1994. An electronic device for long-term snow wetness recording. *Annals of Glaciology* **19**: 104–106.

Dunn C, Hawksford MO. 1993. Distortion immunity of MLS-derived impulse response measurements. *Journal of the Audio Engineering Society* **41**(5): 314–335.

Ellis CR, Pomeroy JW, Link TE. 2013. Modeling increases in snowmelt yield and desynchronization resulting from forest gap-thinning treatments in a northern mountain headwater basin. *Water Resources Research* **49**(2): 936–949. DOI:10.1002/wrcr.20089.

Evje S, Karlsen K. 2009. Global weak solutions for a viscous liquid–gas model with singular pressure law. *Communications on Pure and Applied Analysis* **8**(6): 1867–1894. DOI:10.3934/cpaa.2009.8.1867.

Fang X, Pomeroy JW, Westbrook CJ, Guo X, Minke AG, Brown T. 2010. Prediction of snowmelt derived streamflow in a wetland dominated prairie basin. *Hydrology and Earth System Sciences* **14**(6): 991–1006. DOI:10.5194/hess-14-991-2010.

Farnes PE, Goodison BE, Peterson NR, Richards RP. 1980. Proposed metric snow samplers. *Proceedings of the Western Snow Conference* **48**: 107–119.

Farnes PE, Peterson NR, Goodison BE, Richards RP. 1982. Metrification of manual snow sampling equipment. *Proceedings of the Western Snow Conference* **50**: 120–132.

Ferguson RI. 1999. Snowmelt runoff models. *Progress in Physical Geography* **23**(2): 205–227. DOI:10.1177/030913339902300203.

Fierz C, Armstrong RL, Durand Y, Etchevers P, Greene E, McClung DM, Nishimura K, Satyawali PK, Sokratov SA. 2009. The international classification for seasonal snow on the ground. IHP-VII Technical Documents in Hydrology N°83, IACS Contribution N°1, UNESCO-IHP, Paris. UNESCO: Paris, France.

Goodison BE, Metcalf RA, Wilson RA, Jones K. 1988. The Canadian automatic snow depth sensor: a performance update. *Proceedings of the Western Snow Conference* **56**: 178–181.

Granberg HB, Kingsbury CM. 1984. Tests of new snow density samplers. *Proceedings of the Eastern Snow Conference* **41**: 224–228.

Gray DM, Landine PG. 1988. An energy-budget snowmelt model for the Canadian Prairies. *Canadian Journal of Earth Sciences* **25**: 1292–1303.

Gray DM, Toth B, Zhao L, Pomeroy JW, Granger RJ. 2001. Estimating areal snowmelt infiltration into frozen soils. *Hydrological Processes* **15**(16): 3095–3111. DOI:10.1002/hyp.320.

Grimmett G. 1999. *Percolation*. Springer: Berlin; New York.

Gubler H, Hiller M. 1984. The use of microwave FMCW radar in snow and avalanche research. *Cold Regions Science and Technology* **9**(2): 109–119. DOI:10.1016/0165-232X(84)90003-X.

Helgason W, Pomeroy J. 2012. Problems closing the energy balance over a homogeneous snow cover during midwinter. *Journal of Hydrometeorology* **13**(2): 557–572. DOI:10.1175/JHM-D-11-0135.1.

Huber ML, Perkins RA, Laesecke A, Friend DG, Sengers JV, Assael MJ, Metaxa IN, Vogel E, Mareš R, Miyagawa K. 2009. New international

formulation for the viscosity of H_2O. *Journal of Physical and Chemical Reference Data* **38**(2): 101–125. DOI:10.1063/1.3088050.
Johnson JB. 1982. On the application of Biot's theory to acoustic wave propagation in snow. *Cold Regions Science and Technology* **6**: 49–60.
Jones HG, Pomeroy JW, Walker DA, Hoham RW. 2011. *Snow Ecology: An Interdisciplinary Examination of Snow-Covered Ecosystems*. Cambridge University Press: Cambridge, UK.
Kattelmann R, Dozier J. 1999. Observations of snowpack ripening in the Sierra Nevada, California, U.S.A. *Journal of Glaciology* **45**(151): 409–416.
Kinar NJ. 2013. Acoustic measurement of snow. PhD Thesis, University of Saskatchewan: Saskatoon.
Kinar NJ, Pomeroy JW. 2007. Determining snow water equivalent by acoustic sounding. *Hydrological Processes* **21**(19): 2623–2640. DOI:10.1002/hyp.6793.
Kinar NJ, Pomeroy JW. 2008a. Operational techniques for determining SWE by sound propagation through snow: I. General theory. *Proceedings of the Eastern Snow Conference* **65**: 309–323.
Kinar NJ, Pomeroy JW. 2008b. Operational techniques for determining SWE by sound propagation through snow: II. Instrumentation and testing. *Proceedings of the Eastern Snow Conference* **65**: 19–33.
Kinar NJ, Pomeroy JW. 2009. Automated determination of snow water equivalent by acoustic reflectometry. *IEEE Transactions on Geoscience and Remote Sensing* **47**(9): 3161–3167. DOI:10.1109/TGRS.2009.2019730.
Kováčik J. 1999. Correlation between shear modulus and porosity in porous materials. *Journal of Materials Science Letters* **18**(13): 1007–1010.
Liu W, Weiss S. 2010. *Wideband Beamforming: Concepts and Techniques*. John Wiley and Sons: Chichester, UK.
Lurton X. 2002. *An Introduction to Underwater Acoustics: Principles and Applications*. Springer: New York.
Male DH, Gray DM. 1981. Snowcover ablation and runoff. In *Handbook of Snow: Principles, Processes, Management and Use*. Pergamon Press Canada: Toronto; 360–436.
McGurk BJ, Marsh P. 1995. Flow-finger continuity in serial thick-sections in a melting Sierran snowpack. In *Biogeochemistry of Seasonally Snow-Covered Catchments*, IAHS Publication no. 228. IAHS Press: Wallingford, Oxfordshire, UK; 81–88.
Morland LW, Kelly RJ, Morris RM. 1990. A mixture theory for a phase-changing snowpack. *Cold Regions Science and Technology* **17**: 271–285.
Morris EM, Kelly RJ. 1990. A theoretical determination of the characteristic equation of snow in the pendular regime. *Journal of Glaciology* **36**(123): 179–187.
Mote PW. 2003. Trends in snow water equivalent in the Pacific Northwest and their climatic causes. *Geophysical Research Letters* **30**(12): 1601. DOI:10.1029/2003GL017258.
Ng A, Swanevelder J. 2011. Resolution in ultrasound imaging. *Continuing Education in Anaesthesia, Critical Care & Pain* **11**(5): 186–192. DOI:10.1093/bjaceaccp/mkr030.
Petrenko VF, Whitworth RW. 2002. *Physics of Ice*. Oxford University Press: Oxford ; New York.
Phani KK, Niyogi SK. 1987. Young's modulus of porous brittle solids. *Journal of Materials Science* **22**(1): 257–263. DOI:10.1007/BF01160581.
Pomeroy JW, Gray DM. 1995. Snowcover accumulation, relocation, and management National Hydrology Research Institute Science Report No. 7. National Water Research Institute: Saskatoon, Canada.
Pomeroy JW, Gray DM, Brown T, Hedstrom NR, Quinton WL, Granger RJ, Carey SK. 2007. The Cold Regions Hydrological Model: a platform for basing process representation and model structure on physical evidence. *Hydrological Processes* **21**: 2650–2667.
Raichel DR. 2006. *The Science and Applications of Acoustics*. Springer Science+Business Media: New York.
Rau G, Chaney RC. 1988. Triaxial testing of marine sediments with high gas contents. In *Advanced Triaxial Testing of Soil and Rock*, Issue 977. American Society for Testing and Materials: Philadelphia, PA; 338–352.
Rife DD, Vanderkooy J. 1989. Transfer-function measurement with Maximum-Length Sequences. *Journal of the Audio Engineering Society* **37**: 419–444.
Stoll RD. 1979. Experimental studies of attenuation in sediments. *The Journal of the Acoustical Society of America* **66**(4): 1152–1160. DOI:10.1121/1.383309.
Stoll RD. 1980. Theoretical aspects of sound transmission in sediments. *The Journal of the Acoustical Society of America* **68**(5): 1341–1350. DOI:10.1121/1.385101.
Stoll RD. 1985. Marine sediment acoustics. *The Journal of the Acoustical Society of America* **77**(5): 1789–1799. DOI:10.1121/1.391928.
Stoll RD. 1989. *Sediment Acoustics*. Springer-Verlag: New York; Berlin; Heidelberg.
Stoll RD. 2002. Velocity dispersion in water-saturated granular sediment. *The Journal of the Acoustical Society of America* **111**(2): 785–793. DOI:10.1121/1.1432981.
Stoll RD, Bryan GM. 1970. Wave attenuation in saturated sediments. *The Journal of the Acoustical Society of America* **47**(5B): 1440–1447. DOI:10.1121/1.1912054.
Stoll RD, Kan T-K. 1981. Reflection of acoustic waves at a water–sediment interface. *The Journal of the Acoustical Society of America* **70**(1): 149–156. DOI:10.1121/1.386692.
Tanaka M, Girard G, Davis R, Peuto A, Bignell N. 2001. Recommended table for the density of water between 0 °C and 40 °C based on recent experimental reports. *Metrologia* **38**(4): 301. DOI:10.1088/0026-1394/38/4/3.
Techel F, Pielmeier C. 2011. Point observations of liquid water content in wet snow—investigating methodical, spatial and temporal aspects. *The Cryosphere* **5**(2): 405–418. DOI:10.5194/tc-5-405-2011.
Vanderkooy J. 1994. Aspects of MLS measuring systems. *Journal of the Audio Engineering Society* **42**(4): 219–231.
Wang Y. 2004. Q analysis on reflection seismic data. *Geophysical Research Letters* **31**: L17606.
Wang Y. 2008. *Seismic Inverse Q Filtering*. Blackwell Publishing: Malden, MA; Oxford.
Widess MB. 1973. How thin is a thin bed? *Geophysics* **38**(6): 1176–1180.
Williams MW, Erickson TA, Petrzelka J. 2010. Visualizing meltwater propagation through snow at the centimeter-to-meter scale using a snow guillotine. *Hydrological Processes* **24**(15): 2098–2110.
Willis NJ. 1991. *Bistatic Radar*. Artech House: Boston.
Yankielun N, Rosenthal W, Davis RE. 2004. Alpine snow depth measurements from aerial FMCW radar. *Cold Regions Science and Technology* **40**(1–2): 123–134. DOI:10.1016/j.coldregions.2004.06.005.

